



Article

Spectroscopy and Near-Infrared to Visible Upconversion of Er³⁺ Ions in Aluminosilicate Glasses Manufactured with Controlled Optical Transmission

Daniel Sola ^{1,2,*} , Adrián Miguel ³, Eduardo Arias-Egido ²  and Jose I. Peña ²

¹ Laboratorio de Óptica, Centro de Investigación en Óptica y Nanofísica, Campus Espinardo, Universidad de Murcia, 30100 Murcia, Spain

² Instituto de Nanociencia y Materiales de Aragón, Universidad de Zaragoza-CSIC, 50018 Zaragoza, Spain; earias@unizar.es (E.A.-E.); jipena@unizar.es (J.I.P.)

³ R&D Department, Icer Rail (Knorr-Bremse Group), 31013 Pamplona, Spain; adrian.miguel@knorr-bremse.com

* Correspondence: daniel.sola@um.es

Abstract: In this work we report on the spectroscopic properties and the near-infrared to visible upconversion of Er³⁺ ions in aluminosilicate glasses manufactured by directionally solidification with the laser floating zone technique. Glasses were manufactured in a controlled oxidizing atmosphere to provide them with high optical transmission in the visible spectral range. Absorption and emission spectra, and lifetimes were assessed in both the visible and the near infrared spectral range. Green upconversion emissions of the ²H_{11/2}→⁴I_{15/2} and ⁴S_{3/2}→⁴I_{15/2} transitions at 525 nm and 550 nm attributed to a two-photon process were observed under excitation at 800 nm. Mechanisms responsible for the upconversion luminescence were discussed in terms of excited state absorption and energy transfer upconversion processes. Excitation spectra of the upconverted emission suggest that energy transfer upconversion processes are responsible for the green upconversion luminescence.



Citation: Sola, D.; Miguel, A.; Arias-Egido, E.; Peña, J.I. Spectroscopy and Near-Infrared to Visible Upconversion of Er³⁺ Ions in Aluminosilicate Glasses Manufactured with Controlled Optical Transmission. *Appl. Sci.* **2021**, *11*, 1137. <https://doi.org/10.3390/app11031137>

Received: 23 December 2020

Accepted: 22 January 2021

Published: 26 January 2021

Publisher's Note: MDPI stays neutral with regard to jurisdictional claims in published maps and institutional affiliations.



Copyright: © 2021 by the authors. Licensee MDPI, Basel, Switzerland. This article is an open access article distributed under the terms and conditions of the Creative Commons Attribution (CC BY) license (<https://creativecommons.org/licenses/by/4.0/>).

Keywords: optical properties; erbium; upconversion; aluminosilicate glasses; laser floating zone

1. Introduction

In recent years rare-earth-doped glasses have been subject of intense research as host materials because of their significant optical properties, which make them adequate as infrared and upconversion lasers, optical amplifiers, and active photonic devices [1–9]. In particular, silicate and aluminosilicate glasses present excellent thermal and mechanical properties, and corrosion resistance to be used in practical applications [10–17]. In addition, their maximum phonon energy (~1050 cm⁻¹) is much lower than that of phosphate and borate glasses, ~1300 cm⁻¹ and ~1350 cm⁻¹, respectively, so that quantum efficiency is less influenced by multiphonon relaxation processes [16–19].

Er³⁺ ions are among the most interesting active centers to be studied because of its potential applications in the field of infrared optical amplification related to the radiative efficiency of the ⁴I_{13/2}→⁴I_{15/2} emission at around 1.55 μm [1,2,20]. Furthermore, the rich energy level structure of this rare-earth allows the excitation of the ²H_{11/2}→⁴I_{15/2}, ⁴S_{3/2}→⁴I_{15/2}, and ⁴F_{9/2}→⁴I_{15/2} upconversion emission bands centered at around 530, 550, and 665 nm using wavelengths in the near infrared spectral regions [1,2,21,22]. NIR-to-visible energy conversion mechanism involves the conversion of low-excitation-energy photons into high-energy emitted light in the visible range through non-linear anti-Stokes processes. In addition, these ions can also be used as local ordering probe because of the close relation between their spectroscopic properties and the local structure and bonding at the ion site [23–27].

In a previous work, we reported on how to control the optical transmission of aluminosilicate glasses manufactured departing from commercial glass-ceramics by means of the Laser Floating Zone (LFZ) technique [28]. This technique utilizes an infrared laser source

to create a molten zone in the material from which, by controlling the solidification rates, a new material with controlled microstructure is produced. Surrounding medium during the fabrication process, in terms of oxidizing or reducing atmosphere, can also be controlled. We reported that when the fabrication of these aluminosilicate glasses took place in an oxidizing atmosphere, Ti^{3+} centers contained in the glass turned into Ti^{4+} ions, giving rise to colorless glasses, the transmittance of which ranged 80% in the visible spectral range. Therefore, it was possible to tailor the resulting optical transmission. In this work we have taken advantage of this feature to fabricate erbium-doped glasses in oxidizing atmosphere to give rise to optical active glasses of high optical transmission. Spectroscopic and NIR-to-visible upconversion properties have been studied and the possible excitation mechanisms responsible for this upconversion luminescence were discussed.

2. Materials and Methods

2.1. Sample Fabrication

Glass-ceramic powder was obtained from a commercial glass-ceramic, Ceran Suprema[®], manufactured by Schott. Next, 1 wt% and 4 wt% of Er_2O_3 , ultra-pure 99.99% (Sigma-Aldrich, St. Louis, MO, USA) were mixed and isostatically pressed at 200 MPa for 3 min and sintered at 1200 °C for 12 h to obtain the precursor rods. Glass samples were obtained departing from these erbium-doped glass-ceramic precursors by means of the laser floating zone (LFZ) technique. This manufacturing technique has been described elsewhere [29–31]. Glass samples were obtained at a growth rate of 300 mm/h, which provided both high axial and radial cooling gradients to manufacture glass samples. In addition, the manufacturing process was carried out in a semi-sealed chamber, which allowed working in different atmospheres such as oxygen, nitrogen, and air. Specifically, Er-doped glasses were fabricated in oxygen atmosphere to obtain samples with high optical transmission. Taking into account the theoretical weight percentage the samples were doped with, from now on they will be named as Er1 and Er4.

2.2. Characterization Techniques

Composition of glasses was determined by means of field emission scanning electron microscopy microscope (FESEM) with energy dispersive X-ray detector (EDX) (Carl Zeiss, Jena, Germany). EDX technique allows the determination of most elements present in concentration above 0.1% with an estimated accuracy of $\pm 5\%$.

Absorption spectra were recorded with a Cary 5 spectrophotometer. Steady-state emission were obtained by exciting the sample with an argon laser and a Ti-sapphire ring laser (0.4 cm^{-1} linewidth) in the 770–920 nm spectral range. The fluorescence was analyzed with a 0.25 m Jobin-Yvon monochromator (Horiba, Kyoto, Japan), and the signal was detected by a Hamamatsu R928 photomultiplier and finally amplified by a standard lock-in technique. Infrared emission at 1.5 μm was detected with an extended IR Hamamatsu R5509-72 photomultiplier (Hamamatsu, Hamamatsu-city, Japan).

Lifetime measurements were performed by exciting the samples with a dye laser pumped by a pulsed nitrogen laser and a Ti-sapphire laser, pumped by a pulsed frequency doubled Nd:YAG laser (9 ns pulsewidth) (Coherent, Santa Clara, USA), and detecting the emission with Hamamatsu R928 and R5509-72 photomultipliers (Hamamatsu, Hamamatsu-city, Japan). Data were processed by a Tektronix MDO3104 oscilloscope (Tektronix-Inc, Beaverton, OR, USA).

3. Results

3.1. Compositional Characterization

The composition of the Er-doped glass samples after the fabrication process in an oxygen atmosphere was carried out by EDX microanalysis. Table 1 shows the composition for both the samples. It can be observed that SiO_2 and Al_2O_3 were the majority components of the samples, which also included low percentages of NaO, MgO, TiO_2 , ZrO_2 , and Er_2O_3 . The content of Er^{3+} ions in both glasses was calculated accounting the measured content

of Er_2O_3 and the density of both glasses, 2.35 g/cm^3 and 2.36 g/cm^3 for Er1 and Er4, respectively, resulting in $7.92 \times 10^{19} \text{ at/cm}^3$ for Er1 and $2.71 \times 10^{20} \text{ at/cm}^3$ for Er4.

Table 1. Compositional analysis in at% of the Er-doped samples manufactured in an oxygen atmosphere.

	Na	Mg	Al	Si	Ti	Zr	Er
Er1	0.70	1.81	28.11	65.99	2.00	0.98	0.41
Er4	0.86	1.75	28.12	65.11	1.84	0.89	1.43

3.2. Absorption and Emission Properties

The room temperature absorption spectra were obtained for both samples in the 300–1700 nm range. As an example, Figure 1 shows the absorption spectra as a function of the wavelength for the sample doped with a 4 wt% of Er_2O_3 . The spectrum consists of 10 absorption bands corresponding to the transition from the $^4\text{I}_{15/2}$ ground state to the $^4\text{G}_{11/2}$, $^2\text{H}_{9/2}$, $^4\text{F}_{3/2,5/2}$, $^4\text{F}_{7/2}$, $^2\text{H}_{11/2}$, $^4\text{S}_{3/2}$, $^4\text{F}_{9/2}$, $^4\text{I}_{9/2}$, $^4\text{I}_{11/2}$, and $^4\text{I}_{13/2}$ of Er^{3+} excited states ions [1].

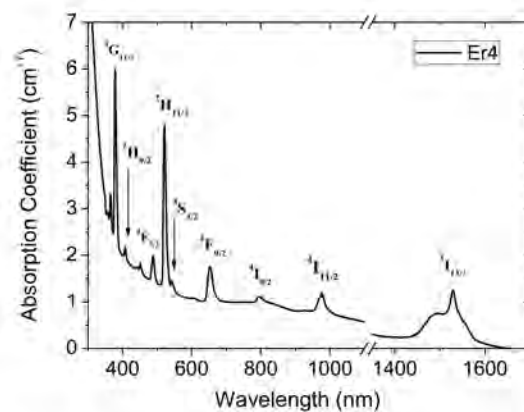


Figure 1. Room temperature absorption spectrum of Er^{3+} in the aluminosilicate glass doped with 4 wt% Er_2O_3 .

Visible emission spectra were obtained at room temperature under excitation of the $^4\text{F}_{7/2}$ level at 488 nm. Multiphonon relaxation processes populated the lower levels resulting in the emission bands observed at around 530, 548, and 660 nm which corresponded to transitions from the $^2\text{H}_{11/2}$, $^4\text{S}_{3/2}$, and $^4\text{F}_{9/2}$ levels to the ground state. Figure 2 shows the emission spectra of both glasses. The main emission corresponded to the $(^2\text{H}_{11/2}, ^4\text{S}_{3/2}) \rightarrow ^4\text{I}_{15/2}$ transition. A weak red emission was also observed from the $^4\text{F}_{9/2}$ level. This level was populated through multiphonon relaxation processes from the $^4\text{S}_{3/2}$ level.

The experimental decays of the luminescence from $^4\text{S}_{3/2}$ and $^4\text{F}_{9/2}$ levels were obtained at room temperature for both glasses under excitation at 488 nm. Table 2 shows the values obtained by a fit to a single exponential function. It can be observed that lifetimes of these levels were found to be similar for both glasses, with values slightly higher for the glass doped with a 1 wt% of Er_2O_3 . As an example, Figure 3 shows the experimental decays from the $^4\text{S}_{3/2}$ and $^4\text{F}_{9/2}$ levels under excitation at 488 nm for the sample doped with 1 wt%. Lifetime was also measured at room temperature for the $^4\text{I}_{13/2}$ level under excitation at 800 nm corresponding to the level $^4\text{I}_{9/2}$. It was also found that lifetime was slightly higher for the glass doped with a 1 wt% of Er_2O_3 . The decay from the $^4\text{I}_{13/2}$ level was found to behave like a perfect single exponential, whereas decays from $^4\text{S}_{3/2}$ and $^4\text{F}_{9/2}$ excited levels slightly deviated from a perfect exponential behavior. The observed lifetimes were in the same order of magnitude than those reported for other silicate and aluminosilicate glasses [10,11,32].

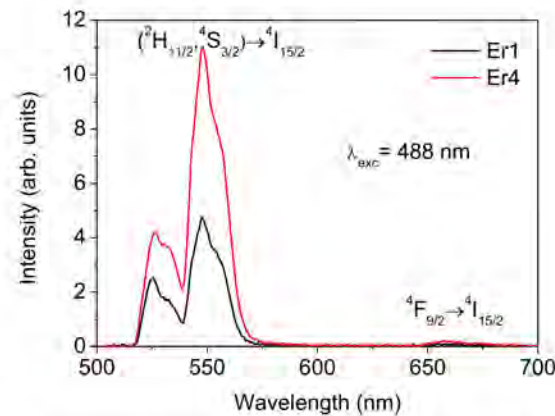


Figure 2. Room temperature emission spectra of the Er-doped aluminosilicate glasses with 1 wt% and 4 wt% under excitation at 488 nm.

Table 2. Lifetimes at room temperature of the $^4S_{3/2}$ and $^4F_{9/2}$ levels obtained under excitation at 488 nm and $^4I_{13/2}$ levels obtained under excitation at 800 nm.

	548 nm ($^4S_{3/2}$) ($\lambda_{exc} = 488$ nm)	660 nm ($^4F_{9/2}$) ($\lambda_{exc} = 488$ nm)	1528 nm ($^4I_{13/2}$) ($\lambda_{exc} = 800$ nm)
Er1	3.60 ± 0.11 μ s	3.06 ± 0.09 μ s	4.91 ± 0.12 ms
Er4	3.20 ± 0.07 μ s	3.17 ± 0.03 μ s	3.01 ± 0.06 ms

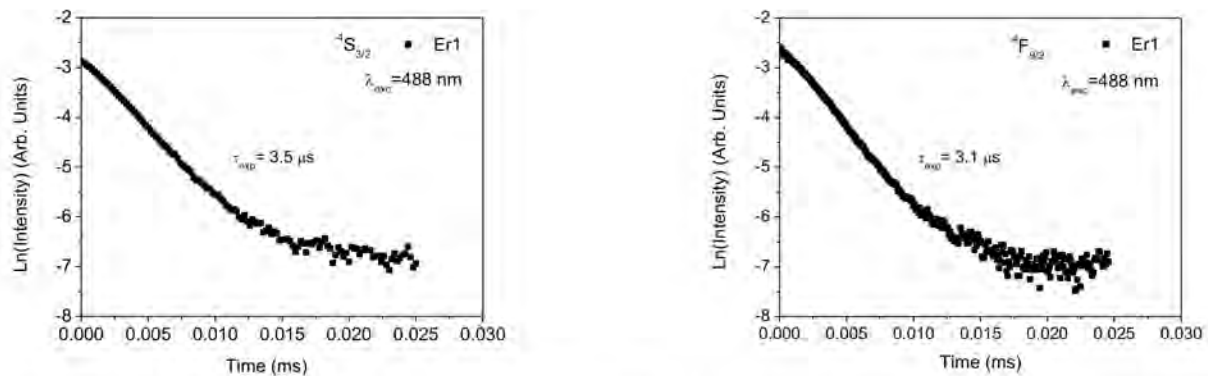


Figure 3. Experimental decays of the $^4S_{3/2}$ and $^4F_{9/2}$ levels of the Er-doped aluminosilicate glasses with 1 wt% under excitation at 488 nm.

The fluorescence spectra at room temperature corresponding to the $^4I_{13/2} \rightarrow ^4I_{15/2}$ transition were measured by exciting the samples at 802 nm. As shown in Figure 4 both samples presented a maximum at around 1528 nm. Effective bandwidth ($\Delta\lambda_{eff}$) was measured according to

$$\Delta\lambda_{eff} = \int \frac{I(\lambda)d\lambda}{I_{max}}, \quad (1)$$

where $I(\lambda)$ is the intensity of the emission spectrum as a function of the wavelength and I_{max} is the peak intensity. It was found that the effective bandwidth increased from 62.5 nm for the sample doped with 1 wt% to 66.3 nm for the sample doped with 4 wt% of Er_2O_3 . These values are larger than those obtained for other silicate and phosphate glasses, the bandwidth of which ranges from 30–40 nm for silicate and 46 nm for phosphate glasses, respectively [33]. This feature is highly significant since broadband amplifiers and tunable lasers require large bandwidth.

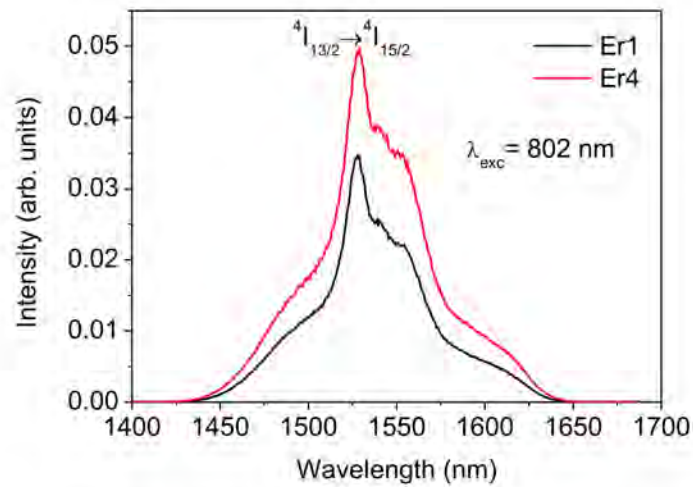


Figure 4. Emission spectra of the ${}^4I_{13/2} \rightarrow {}^4I_{15/2}$ transition for Er-doped aluminosilicate glasses with 1 wt% and 4 wt% under excitation at 802 nm.

In addition to the bandwidth, the stimulated emission cross-section, σ_{em} , is another important parameter that provides information about the optical amplification. This parameter was estimated from the absorption spectra by using the McCumber approach [34], in which the absorption and emission cross-section are related according to

$$\sigma_{em}(\nu) = \sigma_{abs}(\nu) \exp\left[\frac{\epsilon - h\nu}{KT}\right], \quad (2)$$

where σ_{em} and σ_{abs} are the stimulated emission and absorption cross-section, respectively, ν is the photon frequency, h is the Planck constant, K is the Boltzmann constant, and ϵ is the net free energy required to excite one Er^{3+} ion from states ${}^4I_{15/2}$ to ${}^4I_{13/2}$ at temperature T . The absorption cross-section was experimentally obtained and ϵ was determined by using the simplified procedure provided by Miniscalco [35]. The maximum emission cross-sections were found to be $3.51 \times 10^{-21} \text{ cm}^2$ and $4.19 \times 10^{-21} \text{ cm}^2$ at 1530 nm for the samples doped with 1 wt% and 4 wt% of Er_2O_3 , respectively. These values were similar to those found in other aluminosilicate glasses [32]. As an example, Figure 5 shows the absorption and emission cross-section for the sample doped with 4 wt% of Er_2O_3 .

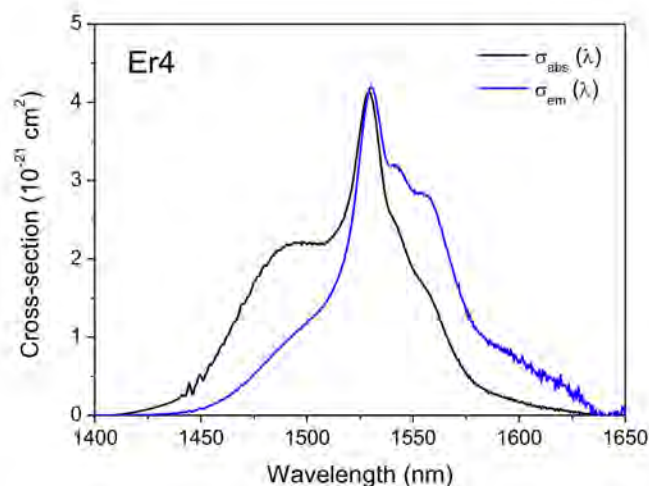


Figure 5. Absorption and emission cross-section for the aluminosilicate glass doped with 4 wt% of Er_2O_3 .

3.3. Infrared to Visible Upconversion

Visible upconversion at room temperature was observed in both samples under continuous laser excitation in resonance with the $^4I_{9/2}$ level, as shown in Figure 6. The observed green emissions correspond to $^2H_{11/2} \rightarrow ^4I_{15/2}$ and $^4S_{3/2} \rightarrow ^4I_{15/2}$ transitions of Er^{3+} ions, which were located approximately at 525 nm and 550 nm, respectively. Nevertheless, red emission corresponding to the $^4F_{9/2} \rightarrow ^4I_{15/2}$ transition was not observed in these glasses. This is due to the fact that the energy gap between levels $^4F_{9/2}$ and $^4I_{9/2}$ is 2264 cm^{-1} and the maximum phonon energy is 1000 cm^{-1} approximately [32].

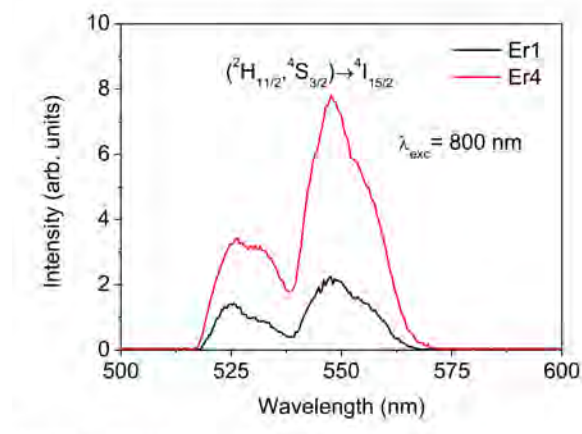


Figure 6. Upconversion emissions at room temperature for Er^{3+} ions in aluminosilicate glasses under excitation at 800 nm.

Excited state absorption (ESA) and energy transfer upconversion (ETU) are the main processes associated to the upconversion emission of rare-earth ions [36]. Excitation mechanisms for populating the $^2H_{11/2}$ and $^4S_{3/2}$ levels under NIR excitation were investigated by studying the upconversion emission intensity I_{up} as a function of the infrared excitation power I_{IR} . It is well-known that upconversion emission intensity increases proportionally to the n th power of the infrared excitation power according to the relation $I_{up} \propto (I_{IR})^n$, where n is the number of photons involved in the pumping mechanism. Figure 7 shows the logarithmic plot of the green upconversion intensity I_{up} compared to the excitation power I_{IR} under excitation at 800 nm for both glass samples. Linear fit allowed determining the n -values, resulting in 1.47 and 1.52 for Er1 and Er4, respectively. Slope values below two indicates a saturation of the intermediate levels [37]. These results confirm that a two-photon step was involved in the upconversion process to populate the emitting levels.

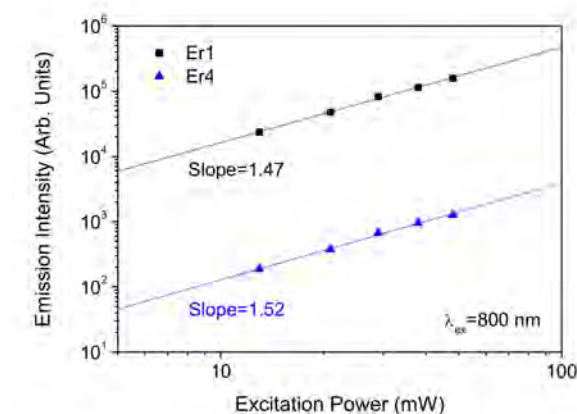


Figure 7. Dependence of green upconversion emission intensity on excitation power for Er^{3+} ions under excitation at 800 nm.

Possible mechanisms accounting for green upconversion emission under 800 nm excitation is presented in Figure 8. Green upconverted emission requires the population of levels with at least the energy of the ${}^2\text{H}_{11/2}$ level or higher. The ${}^4\text{I}_{9/2}$ level is resonantly excited by the pumping wavelength at 800 nm. Next, the thermalized levels ${}^2\text{H}_{11/2}$ and ${}^4\text{S}_{3/2}$ can be populated by means of two ESA processes or two ETU. On the first ESA, labelled as ESA1, a non-radiative relaxation from the ${}^4\text{I}_{9/2}$ level to the lower ${}^4\text{I}_{11/2}$ level is produced, from which the absorption of one photon populates the ${}^4\text{F}_{3/2,5/2}$ level, followed by a non-radiative de-excitation to the ${}^2\text{H}_{11/2}$ and ${}^4\text{S}_{3/2}$ levels. On the second ESA, labelled as ESA2, an additional non-radiative relaxation from the ${}^4\text{I}_{11/2}$ level to the ${}^4\text{I}_{13/2}$ level is produced. Then, the absorption of one photon promotes the Er^{3+} ions to the ${}^2\text{H}_{11/2}$ and ${}^4\text{S}_{3/2}$ levels. These two processes involve only one Er^{3+} ion. Nevertheless, two upconversion mechanisms involving the interaction of two nearby Er^{3+} ions in the ${}^4\text{I}_{11/2}$ level and entailing an energy transfer are possible. In the first ETU, denoted as I, the mechanism can be described as $\text{Er}^{3+}({}^4\text{I}_{11/2}) + \text{Er}^{3+}({}^4\text{I}_{11/2}) \rightarrow \text{Er}^{3+}({}^4\text{I}_{15/2}) + \text{Er}^{3+}({}^4\text{F}_{7/2})$, followed by a non-radiative de-excitation to the ${}^2\text{H}_{11/2}$ and ${}^4\text{S}_{3/2}$ levels. The second ETU, denoted as II, can be described as $\text{Er}^{3+}({}^4\text{I}_{11/2}) + \text{Er}^{3+}({}^4\text{I}_{13/2}) \rightarrow \text{Er}^{3+}({}^4\text{I}_{15/2}) + \text{Er}^{3+}({}^2\text{H}_{11/2}, {}^4\text{S}_{3/2})$.

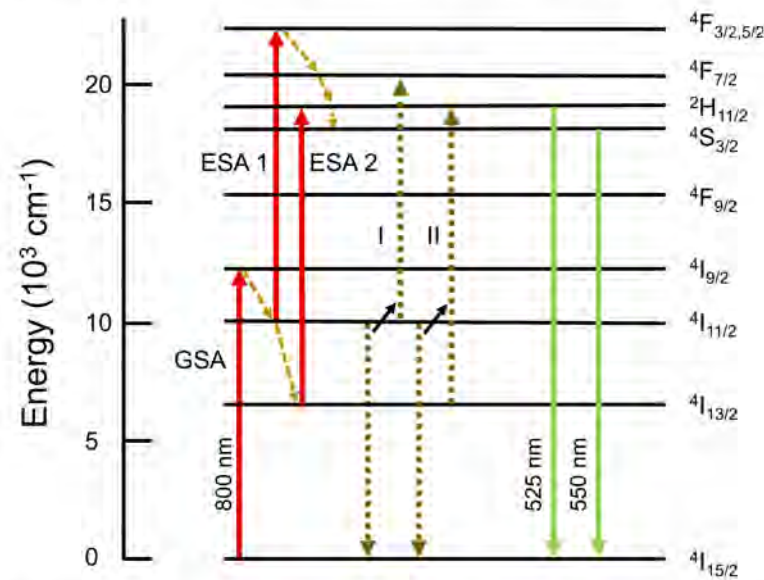


Figure 8. Energy level of Er^{3+} ions in aluminosilicate glass and possible upconversion mechanisms under excitation at 800 nm.

A method to distinguish between ESA and ETU mechanisms is provided by the excitation spectra of the upconverted luminescence [38]. In ESA processes upconversion excitation spectra are the result of excited state absorption and the one photon absorption. In ETU, excitation spectra are proportional to the square of the ground state absorption. Hence, excitation spectra of the upconversion green emission were performed in the ${}^4\text{S}_{3/2} \rightarrow {}^4\text{I}_{15/2}$ transition at 550 nm in both Er-doped aluminosilicate glasses. Figure 9 shows these spectra for the sample doped with a 4 wt%. It can be observed that both excitation and absorption spectra are similar. This behavior was also observed for the sample doped with a 1 wt%. Consequently, upconversion mechanisms were due to energy transfer upconversion processes.

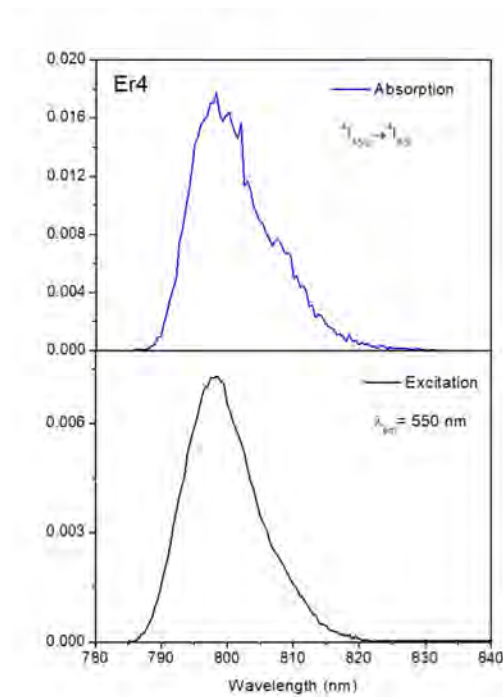


Figure 9. Excitation spectra of upconverted green emission from the ${}^4S_{3/2}$ level and square of the one photon absorption spectra of the aluminosilicate glass doped with 4 wt% Er_2O_3 .

4. Conclusions

Directionally solidified Er-doped aluminosilicate glasses were manufactured by the laser floating zone in a controlled oxidizing atmosphere to provide them with a high optical transmission in the visible spectral range. The infrared and visible emissions were assessed at room temperature. Infrared emission corresponding to the ${}^4I_{13/2} \rightarrow {}^4I_{15/2}$ transition at 1528 nm presented an effective bandwidth nearly 30 nm broader than other silicate glasses, which makes them suitable for broadband amplifiers. The visible emission was dominated by the green emission corresponding to the ${}^2H_{11/2}$ and ${}^4S_{3/2}$ levels. Lifetimes from levels ${}^4S_{3/2}$ and ${}^4F_{9/2}$ at room temperature under excitation at 488 nm were found to be similar for both glasses, whereas lifetime from the ${}^4I_{13/2}$ level was found to be shorter for the glass with the higher content of Er^{3+} ions.

NIR-to-visible upconversion of Er^{3+} ions in these glasses under excitation at 800 nm presented intense green emissions corresponding to ${}^2H_{11/2} \rightarrow {}^4I_{15/2}$ and ${}^4S_{3/2} \rightarrow {}^4I_{15/2}$ transitions placed at 525 nm and 550 nm which were attributed to a two-photon process. Nevertheless, red upconversion emission for the ${}^4F_{9/2} \rightarrow {}^4I_{15/2}$ transition was not observed due to the high maximum phonon energy. Excitation spectra of the upconverted luminescence from the ${}^4S_{3/2}$ level suggests the energy transfer upconversion as the mechanism responsible for the upconversion process in these glasses.

Author Contributions: D.S. conceived and planned the experiments. D.S., A.M., and E.A.-E. carried out the experiments. D.S., A.M. and E.A.-E., J.I.P. contributed to the interpretation of the results and provided critical feedback. D.S. wrote the paper with input from all authors. All authors have read and agreed to the published version of the manuscript.

Funding: This research was funded by the PIT2 program of the University of Murcia's own research plan. Fundación Séneca grant No 20647/JLI/18 and European Union's Horizon 2020 research and innovation programme under the Marie Skłodowska-Curie IF No 795630 are also acknowledged.

Institutional Review Board Statement: Not applicable.

Informed Consent Statement: Not applicable.

Data Availability Statement: All data generated or analyzed during this study are included in this published article. Presented data are also available on request from the corresponding author.

Conflicts of Interest: The authors declare no conflict of interest.

References

- Henderson, B.; Imbusch, G.F. *Optical Spectroscopy of Inorganic Solids*; Oxford University Press: Oxford, UK, 1989.
- Hirao, K.; Mitsuyu, T.; Si, J.; Qiu, J. *Active Glass for Photonic Devices: Photoinduced Structures and Their Application*; Springer: Berlin/Heidelberg, Germany, 2001.
- Campbel, J.H.; Hayden, J.S.; Marker, A.J. High-power solid-state lasers from a laser glass perspective. *Int. J. Appl. Glass Sci.* **2011**, *2*, 3. [[CrossRef](#)]
- Sola, D.; Balda, R.; Peña, J.I.; Fernández, J. Site-selective laser spectroscopy of Nd³⁺ ions in 0.8CaSiO₃-0.2Ca₃(PO₄)₂ biocompatible eutectic glass-ceramics. *Opt. Express* **2012**, *20*, 10701–10711. [[CrossRef](#)] [[PubMed](#)]
- Sola, D.; Martínez de Mendivil, J.; Vázquez de Aldana, J.R.; Lifante, G.; Balda, R.; de Aza, A.H.; Pena, P.; Fernández, J. Stress-induced buried waveguides in the 0.8CaSiO₃-0.2Ca₃(PO₄)₂ eutectic glass doped with Nd³⁺ ions. *Appl. Surf. Sci.* **2013**, *278*, 289. [[CrossRef](#)]
- Wang, Y.; Xu, W.; Cui, S.; Xu, S.; Yin, Z.; Song, H.; Zhou, P.; Liu, X.; Xu, L.; Cui, H. Highly improved upconversion luminescence in NaGd(WO₄)₂:Yb³⁺/Tm³⁺ inverse opal photonic crystals. *Nanoscale* **2015**, *7*, 1363. [[CrossRef](#)] [[PubMed](#)]
- Martínez de Mendivil, J.; Sola, D.; Vázquez de Aldana, J.R.; Lifante, G.; de Aza, A.H.; Pena, P.; Peña, J.I. Ultrafast direct laser writing of cladding waveguides in the 0.8CaSiO₃-0.2Ca₃(PO₄)₂ eutectic glass doped with Nd³⁺ ions. *J. Appl. Phys.* **2015**, *117*, 4906963. [[CrossRef](#)]
- Martín Rodríguez, E.; López-Peña, G.; Montes, E.; Lifante, G.; García Solé, J.; Jaque, D.; Díaz-Torres, L.A.; Salas, P. Persistent luminescence nanothermometer. *Appl. Phys. Lett.* **2017**, *111*, 91901. [[CrossRef](#)]
- Carvalho, D.O.; Kassab, L.R.P.; Del Cacho, V.D.; da Silva, D.M.; Alayo, M.I. A review on pedestal waveguides for low loss optical guiding, optical amplifiers and nonlinear optics applications. *J. Lumin.* **2018**, *203*, 135. [[CrossRef](#)]
- Devarajulu, G.; Ravi, O.; Reddy, C.M.; Ali Ahamed, S.Z.; Raju, B.D.P. Spectroscopic properties and upconversion studies of Er³⁺-doped SiO₂-Al₂O₃-Na₂CO₃-SrF₂-CaF₂ oxyfluoride glasses for optical amplifier applications. *J. Lumin.* **2018**, *194*, 499. [[CrossRef](#)]
- Lifante, G.; Martínez de Mendivil, J.; He, R.; Cantelar, E.; Ortega San Martín, L.; Sola, D. Transition probabilities of Er³⁺ ions in alumino-silicate glasses. *J. Lumin.* **2018**, *203*, 305–312. [[CrossRef](#)]
- Kohli, J.; Shelby, J.E. Rare-earth Aluminosilicate Glasses. *J. Am. Ceram. Soc.* **1990**, *73*, 39–42.
- Hyatt, M.J.; Day, D.E. Glass properties in the yttria-alumina-silica system. *J. Am. Ceram. Soc.* **1987**, *70*, 283–287. [[CrossRef](#)]
- Vomacka, P.; Babushkin, O. Yttria-alumina—silica glasses with addition of zirconia. *J. Eur. Ceram. Soc.* **1995**, *15*, 921–928. [[CrossRef](#)]
- Lin, S.L.; Hwang, C.S. Structures of CeO₂-Al₂O₃-SiO₂ glasses. *J. Non-Cryst. Solids* **1996**, *202*, 61–67. [[CrossRef](#)]
- Erbe, E.M.; Day, D.E. Properties of Sm₂O₃-Al₂O₃-SiO₂ glasses for in vivo applications. *J. Am. Ceram. Soc.* **1990**, *73*, 2708–2713. [[CrossRef](#)]
- Sainz, M.A.; Osendi, M.I.; Miranzo, P. Protective Si–Al–O–Y glass coatings on stainless steel in situ prepared by combustion flame spraying. *Surf. Coat. Technol.* **2008**, *202*, 1712–1717. [[CrossRef](#)]
- Cao, R.; Lu, Y.; Tian, Y.; Huang, F.; Xu, S.; Zhang, J. Spectroscopy of thulium and holmium co-doped silicate glasses. *Opt. Mater. Express* **2016**, *6*, 2252. [[CrossRef](#)]
- Li, M.; Guo, Y.; Bai, G.; Tian, Y.; Hu, L.; Zhang, J. 2 μm luminescence and energy transfer characteristics in Tm³⁺/Ho³⁺ co-doped silicate glass. *J. Quant. Spectrosc. Radiat.* **2013**, *127*, 70. [[CrossRef](#)]
- Dorosz, D.; Zmojda, J.; Kochanowicz, M. Investigation on broadband near-infrared emission in Yb³⁺/Ho³⁺ co-doped antimony-silicate glass and optical fiber. *Opt. Mater.* **2013**, *35*, 2577. [[CrossRef](#)]
- Rodríguez-Mendoza, U.R.; Lalla, E.A.; Cáceres, J.M.; Rivera-López, F.; León-Luís, S.F.; Lavín, V. Optical characterization, 1.5 μm emission and IR-to-visible energy upconversion in Er³⁺-doped fluorotellurite glasses. *J. Lumin.* **2011**, *131*, 1239–1248. [[CrossRef](#)]
- Carnall, W.T.; Fields, P.R.; Rajnak, K. Electronic energy levels in the trivalent lanthanide aquo ions. I. Pr³⁺, Nd³⁺, Pm³⁺, Sm³⁺, Dy³⁺, Ho³⁺, Er³⁺, and Tm³⁺. *J. Chem. Phys.* **1968**, *49*, 4424. [[CrossRef](#)]
- Weber, M.J. Glass for Neodymium glasses. *J. Non-Cryst. Solids* **1980**, *42*, 189. [[CrossRef](#)]
- Tanabe, S.; Ohyagi, T.; Soga, N.; Hanada, T. Compositional dependence of Judd-Ofelt parameters of Er³⁺ ions in alkali-metal borate glasses. *Phys. Rev. B* **1992**, *46*, 3305. [[CrossRef](#)] [[PubMed](#)]
- Ebendor-Heidepriem, H.; Ehrhart, D.; Bettinelli, M.; Speghini, A. Effect of glass composition on Judd-Ofelt parameters and radiative decay rates of Er³⁺ in fluoride phosphate and phosphate glasses. *J. Non-Cryst. Solids* **1998**, *240*, 66. [[CrossRef](#)]
- Quintas, A.; Majérus, O.; Lenoir, M.; Caurant, D.; Klementiev, K.; Webb, A. Effect of alkali and alkaline-earth cations on the neodymium environment in a rare-earth rich aluminoborosilicate glass. *J. Non-Cryst. Solids* **2008**, *354*, 98. [[CrossRef](#)]
- Sola, D.; Conejos, D.; de Mendivil, J.M.; Ortega-San-Martín, L.; Lifante, G.; Peña, J.I. Directional solidification, thermo-mechanical and optical properties of (Mg_xCa_{1-x})₃Al₂Si₃O₁₂ glasses doped with Nd³⁺ ions. *Opt. Express* **2015**, *23*, 26356. [[CrossRef](#)]
- Arias-Egido, E.; Sola, D.; Pardo, J.A.; Martínez, J.I.; Cases, R.; Peña, J.I. On the control of optical transmission of aluminosilicate glasses manufactured by the laser floating zone technique. *Opt. Mater. Express* **2016**, *6*, 2413–2421. [[CrossRef](#)]
- Llorca, J.; Orera, V.M. Directionally-solidified eutectic ceramic oxides. *Prog. Mater. Sci.* **2006**, *51*, 711–809. [[CrossRef](#)]
- Sola, D.; Ester, F.J.; Oliete, P.B.; Peña, J.I. Study of the stability of the molten zone and the stresses induced during the growth of Al₂O₃-Y₃Al₅O₁₂ eutectic composite by the laser floating zone technique. *J. Eur. Ceram. Soc.* **2011**, *31*, 1211–1218. [[CrossRef](#)]

31. Ester, F.J.; Sola, D.; Peña, J.I. Thermal stresses in the $\text{Al}_2\text{O}_3\text{-ZrO}_2(\text{Y}_2\text{O}_3)$ eutectic composite during the growth by the laser floating zone technique. *Bol. Soc. Esp. Ceram.* **2008**, *47*, 352–357. [[CrossRef](#)]
32. Balda, R.; Merino, R.I.; Peña, J.I.; Orera, V.M.; Arriandiaga, M.A.; Fernández, J. Spectroscopic properties and frequency upconversion of Er^{3+} -doped $0.8\text{CaSiO}_3\text{-}0.2\text{Ca}_3(\text{PO}_4)_2$ eutectic glass. *Opt. Mater.* **2009**, *31*, 1105–1108. [[CrossRef](#)]
33. Ding, Y.; Jiang, S.; Hwang, B.; Luo, T.; Peyghambariana, N.; Himei, Y.; Ito, T.; Miura, Y. Spectral properties of erbium-doped lead halotellurite glasses for 1.5 μm broadband amplification. *Opt. Mater.* **2000**, *15*, 123–130. [[CrossRef](#)]
34. McCumber, D. Einstein Relations Connecting Broadband Emission and Absorption Spectra. *Phys. Rev.* **1964**, *136*, 957. [[CrossRef](#)]
35. Miniscalco, W.J.; Quimby, R.S. General procedure for the analysis of Er^{3+} cross sections. *Opt. Lett.* **1991**, *16*, 258–260. [[CrossRef](#)] [[PubMed](#)]
36. Wright, J.C. Up-conversion and excited state energy transfer in rare-earth doped materials. In *Radiationless Processes in Molecules and Condensed Phases*; Springer: Berlin/Heidelberg, Germany, 1976; pp. 239–295.
37. Pollnau, M.; Gamelin, D.R.; Lüthi, S.R.; Güdel, H.U. Power dependence of upconversion luminescence in lanthanide and transition-metal-ion systems. *Phys. Rev. B* **2000**, *61*, 3337–33346. [[CrossRef](#)]
38. Balda, R.; Garcia-Adeva, A.J.; Voda, M.; Fernández, J. Upconversion processes in Er^{3+} -doped KPb_2Cl_5 . *Phys. Rev. B* **2004**, *69*, 205203-1–205203-8. [[CrossRef](#)]